Testing ground based observations of wave activity in the (lower and upper) atmosphere as possible (complementary) indicators of streamer events

Michal Kozubek[1], Lisa Kuchelbacher[2], Jaroslav Chum[1], Tereza Sindelarova[1], Franziska Trinkl[2, a], Katerina Podolska[1]~~,~~

[1]Institute of Atmospheric Physics CAS, Bocni II 1401, Prague, 14100, Czech Republic

~~2~~[2] Earth Observation Center, Deutsches Zentrum für Luft- und Raumfahrt~~,~~82234 Weßling, Germany

[a] now at Karlsruhe Institute of Technology (KIT), Institute of Meteorology and Climate Research, Karlsruhe, Germany

Correspondence: Michal Kozubek, kom@ufa.cas.cz

Keywords: gravity waves, streamer events, infrasound, Doppler measurements

Abstract: For a better understanding of atmospheric dynamics, it is very important to know the general condition (dynamics and chemistry) of the atmosphere. Planetary waves (PWs) are global scale waves, which are well-known as main drivers of the large-scale weather patterns in mid-latitudes on time scales from several days up to weeks in the troposphere. When PWs break, they often cut pressure cells off the jet stream. A specific example are so-called streamer events, which occur predominantly in the lower stratosphere at mid- and high-latitudes. For streamer events we check, ~~if~~whether there are any changes of gravity wave (GW) or infrasound characteristics related to these events in ionospheric and surface measurements (continuous Doppler soundings, ~~array~~two arrays of microbarometers) in the Czech Republic. ~~First order signatures of streamer events~~Different phenomena were ~~not~~ identified in infrasound ~~data~~arrival parameters at the respective surface infrasound stations ~~WBCI~~ and ~~PVCI~~also during the respective analysed streamer events. The streamers signatures in infrasound observations are variable, because the location of the events and their impact on the tropopause – lower stratosphere region differs from event to event. Supplementary ground-based measurements of GW using the WBCI array in the troposphere showed that GW propagation azimuths were more random during streamer and streamer-like events compared to those observed during calm conditions. GW propagation characteristics observed

in the ionosphere by continuous Doppler soundings during streamer events did not differ from those expected for the given time period.

1) Introduction

For a better comprehension of climate change it is fundamentally important, how well we understand the climate system in general, and the dynamics of the atmosphere in particular. The ~~dynamic~~dynamical processes relevant in this context in the atmosphere take place over a comparatively wide range of scales in space and time. They include in particular both, planetary and gravity waves. Planetary waves are the main drivers of the extratropical circulation. When they break, they lead to an irreversible exchange of air masses between the equatorial and polar region due to an amplification of their amplitudes (e.g. McIntyre & Palmer, 1983~~,~~; Polvani & Plumb~~ ~~,1992). In the~~ upper troposphere /~~ lower stratosphere ozone can be used as a tracer for these large-scale motions, as it has a comparatively long life-time. When planetary waves break tropical air masses of low ozone concentration are mixed poleward into the sourrounding atmosphere of the mid and higher latitudes (e.g. Leovy et al~~.~~., 1985). ~~Streamer events do not have~~

The term "streamer" lacks a ~~unique~~precise definition~~ in literature, which makes them difficult to detect objectively. As those streamer events originate~~, as noted by ~~planetary wave dynamics, the spatio-temporal characteristics are closely linked.~~Krüger et al. (2005). They ~~persist for days to weeks and extend over a region~~discuss various aspects of ~~several 1000 km. Often smaller scale air masses detach from these~~ streamers~~ and are irreversibly mixed into~~, including their impact on mixing and the divergent definitions associated with them. Offermann et al. (1999) describe streamers as large-scale tongue-like structures formed by the meridional deflection of air masses. Streamers are characterized by irreversible mixing of air masses between equatorial and polar regions which is why they might be linked to planetary wave breaking (Waugh, 1993). Eyring et al. ~~higher latitudes. It is found~~(2003) give a climatology of the seasonal and geographical distribution of streamer events. They show, that streamers ~~mainly~~often occur ~~at the transition zone from~~ over the Northern Atlantic ~~to Europe and also, but less often, from the Northern Pacific to Northern America (e.g.~~and can be identified by either high NO_2 or low ozone concentration,~~ Eyring et al. 2002, James 1998)~~ which is why we ~~will focus on the Northern Atlantic / European transition region. Measurements in these regions are – due to lack of ground- or ship-based~~select streamers by total ozone column measurements~~ in~~. They show that streamer events occur most ~~cases only available from satellites~~often during winter and least during July and August in the Northern Hemisphere. During a streamer event the wind field changes rather strong over a comparatively small distance. Since a streamer event shows a strong wind shear at its flanks, it is expected that it excites GW (e.g. Kramer et al., 2015 and 2016 or Peters et al., 2003). ~~Therefore, our focus will be on GW periods.~~

It is well-known that enhanced wind gradients or anticyclones can lead to the excitation of gravity waves (GW) in the atmosphere (e.g. Pramitha et al., 2015~~,~~; Kai et al., 2010~~,~~; Kramer et al., 2015, 2016 and Gerlach et al., 2003). GW have typical vertical wavelengths from a few 100 m to several kilometres (Wüst & Bittner, 2006), and horizontal wavelenghts over tens of km (Wüst et al., 2018), and longer (Rauthe et al., 2006); their fluctuations in the upper troposphere / lower stratosphere typically show amplitudes of 5–10 m/s at maximum (e.g., Kramer et al., 2015). Those waves transport energy and momentum horizontally and vertically through the atmosphere and deposit them especially in the stratosphere and mesosphere but also above and below this height region. The propagation of GWs is strongly dependent on the wind conditions in the stratosphere since the wind ~~field~~speed of the middle atmosphere (10~~-~~–100 km) reaches its maximum there. That is why monitoring waves in upper parts of the atmosphere, e.g. based on Doppler observations in the ionosphere, can provide ~~us~~ additional information about stratospheric conditions (for details see Fritts and Alexander, 2003).

Using pressure recordings at a microbarograph array, GWs and infrasound at the ground can be observed. Ground based observations of GWs at a large aperture microbarograph array are utilized in the present study as an independent data source for the analysis of GW activity during streamer events. Infrasound propagation is influenced by wind and temperature fields in the atmosphere. Three regions play an important role in long-distance infrasound propagation: (1) the lower thermosphere; (2) the stratosphere; (3) the jet stream near the tropopause and inversion layers in the troposphere (Evers and Haak, 2010). Infrasound observed at the ground and emitted by distant sources mostly propagates in the stratospheric waveguide (Ceranna et al., 2019). The thermospheric waveguide is not as efficient as the stratospheric waveguide in the long-range infrasound propagation. Besides signal loss due to geometrical spreading, infrasound absorption is important in the upper atmosphere (Bittner et al., 2010). Infrasound absorption is proportional to the frequency; higher frequencies, particularly those above 1 Hz undergo stronger absorption in the thermosphere (Sutherland and Bass, 2004). Signal attenuation is low at frequencies of the order of $10^{-3} – 10^{-2}$ Hz (Blanc, 1985; Georges, 1968).

A number of case studies have proved that stratospheric dynamics can be deduced from microbarograph measurements at the ground (Assink et al., 2014; Blixt et al., 2019; Evers and Siegmund, 2009; Evers et al., 2012; Garcès et al., 2004; Le Pichon and Blanc, 2005; Le Pichon et al., 2006 and 2009; Smets and Evers, 2014). Streamer events are significant transient disturbances to circulation patterns in the tropopause/lower stratosphere region; modifications of the stratospheric waveguide can therefore be expected. A feasibility study on utilisation of ground infrasound measurements in research of streamer events ~~will be~~is performed~~ using data from two infrasound stations in the Czech Republic.~~. Its aim ~~will be~~is to identify ~~possible first order ~~phenomena in infrasound detections related to the streamers~~ – significant ~~; we focus on deviations ~~in infrasound arrival parameters with focus on ~~of the azimuth of signal ~~arrival~~arrivals, trace velocity, signal amplitude, and frequency~~ fluctuations.~~. The dedicated studies demonstrated that from the observed signal trace velocity, information about the signal refraction height can be derived (Lonzaga, 2015). If ~~an occurrence of such phenomena was proved during streamer events~~the source of received signals is well defined in time and ~~if attributes of the phenomena were generally applicable, notification~~space, mean atmospheric cross-winds along the signal propagation path can be estimated from back-azimuth deviations and time of ~~a streamer event could be based on a routine operational evaluation~~signal propagation (Blixt et al., 2019). Fluctuations of ~~infrasound detections as such (without using complementary datasets) and ground based infrasound measurements could serve as a quick indicator~~signal frequency and amplitude are, besides variability of ~~streamers.~~the signal source influenced by atmospheric filtering (Sutherland and Bass, 2004).

Our study will focus on possible utilization Doppler sounding and microbarographs for description and analysis of GW behaviour and propagation in the stratosphere.

The structure of the paper is as ~~follow~~follows: After introduction the description of the used dataset and method can be found in the second section. Then we describe our results and in the last section we discuss the possible connection to previous studies.

2) Data and methods

The ~~data basis of the~~ selection of ~~the~~ streamer events ~~are~~ is based on the visual inspection of global maps of total ozone column ~~measurements~~ (TO3~~) which are available as~~), accessible through a service provided by DLR ~~(https://atmos.eoc.dlr.de/). TO3 is retrieved~~(https://atmos.eoc.dlr.de/) measured by the Tropospheric Monitoring Instrument (TROPOMI) ~~on~~aboard the Sentinel 5 Precursor (S5P) mission. ~~Whenever no data by~~See Veefkind et al., 2012 for details about TROPOMI/S5P~~.~~. In cases where TROPOMI/S5P data is ~~available, TO3~~unavailable, measurements ~~of~~from the Global Ozone Monitoring Experiment-2 (GOME-2) on the Metop series of satellites ~~is considered.~~are utilized. Both instruments ~~are~~operate in a nadir-viewing configuration on ~~a~~ near-polar sun-synchronous ~~orbit. TROPOMI on S5P was launched in 2017 and has a spatial resolution of 7x7 km^2 with a daily global coverage and a repeat cycle of 17 days (Veefkind et al. 2012). Details on TO3~~ orbits. Further specifics regarding TO3 measurements by TROPOMI/S5P are ~~given~~elaborated by Spurr et al. (2022). The TO3 retrieval process is ~~based on~~built upon the predecessor instrument's processor ~~of the previous GOME instrument:~~, with GOME-2 on Metop-AB ~~was launched in 2006. It has a spatial resolution of 80x40 km^2 and almost a daily global coverage with a repeat cycle of 29 days. See~~, see Munro et al. (2006) and Munro et al. (2016 ~~for an overview of the instrument and data processing. Details of the~~). For detailed information on the GOME-2 retrieval algorithm ~~can be found in~~, refer to Loyola et al. (2011).

~~Streamer events are selected manually for this study, as no distinct definition exists. As planetary waves are permanently disturbing the atmospheric dynamic, especially smaller scale streamers can be observed almost every day and the differentiation between streamer events and calm~~We define a streamer as such when the ozone column concentration of the finger-like structure above the Northern Atlantic/Western Europe is lower than 300 DU and persists for at least 3 days. The longitudinal extension is of approx. 15 to 30 degrees in the mid-latitudes (between 30 to 70°N). The northernmost point of a streamer exceeds 50°N. Fig. 1 shows a streamer event above the Northern Atlantic, indicated by the blue color which represent the low ozone concentrations. The streamer shown in Fig. 1 reaches latitudes beyond 70°N, which indicates a large example. At the western and eastern flanks of the streamer, the ozone concentration exceeds 350 DU, defining distinct boundaries. This is also visible in Fig. 1 represented by the green colors at the eastern coast of Northern America and western Europe. So, there is a gradient of the ozone concentration of about 50 DU / 5°. Furthermore, the streamer exhibits a discernible pattern of circulation, with air masses being meridionally deflected, contributing to its formation and maintenance. These air masses, characterized by their movement from south to north at the eastern flank and from north to south at the western flank, play a significant role in the streamer's dynamics. This is the reason why equatorial low ozone concentration is transported northward. In contrast, the calm periods, representing the opposite dynamic situation to the streamer events, are characterized by only very few meridionally deflected air masses. During these periods, the ozone concentration in the mid-latitudes above the Northern Atlantic is consistently higher than 350 DU, indicating stable atmospheric conditions and minimal perturbations in the ozone distribution. An example for a calm period is shown in Fig. 2.

The streamer events are selected by eye for this study (results see **Error! Reference source not found.**) considering the TO3 global maps from January 2020 and March 2021. As planetary waves are permanently disturbing the atmospheric dynamic of the higher troposphere / lower stratosphere, especially smaller scale streamers can be observed almost every day and the identification of streamer events becomes subjective. We therefore focus on few events which are comparatively strong in their evolution from our perspective. Moreover, we focus on streamer events above the Northern Atlantic. Whenever another streamer event occurs ~~at~~somewhere other than over the ~~same time at another latitudinal~~Northern Atlanic region with comparable ~~spatio-temporal~~spatiotemporal extent, we do not consider this date as a streamer event. We assume that the effects of the streamer superimpose and a distinct backtrack to the streamer over the Northern Atlantic will not be possible. This means, that the analysis of the streamer events can be blurred to some extent.

We consider dates from January 2020 to April 2021. In general, planetary waves drive the Brewer Dobson Circulation in the stratosphere during winter and ozone-poor airmasses are transported northward. Streamer events are therefore detected between September and March. The streamer events are distinguished if they have a large spatial size, high intensity (low TO3 concentration) and if air masses are irreversibly mixed into the surrounding atmosphere. All the selected events persist for several days, but no longer than 10 days. ~~The streamer events given in table 1 (left) are selected manually, by the given criterions.~~

To evaluate ~~weather~~whether streamer events effect the smaller-scale atmospheric dynamics, calm events are identified as well by subjective ~~criterions~~criteria. These events serve as a reference to streamer events, as large-scale ~~dynamics~~spatial structures are hardly visible in the TO3. The events are selected when the ozone concentration shows a ~~strong~~ meridional gradient from the equator to polar region on the Northern Hemisphere with almost no longitudinal variation. The examples of calm atmospheric dynamics are listed in ~~table~~Table 1 (right).

Streamer events		**Calm periods**	
From	**To**	**From**	**To**
06.02.2020	10.02.2020	02.03.2020	08.03.2020
11.2.2020	13.2.2020	09.03.2020	14.03.2020
31.08.2020	03.09.2020	28.03.2020	10.04.2020
05.09.2020	11.09.2020	19.04.2020	27.05.2020
03.11.2020	07.11.2020	9.11.2020	15.11.2020
21.11.2020	25.11.2020	12.12.2020	22.12.2020
23.02.2021	27.02.2021	30.12.2020	06.01.2021
09.03.2021	12.03.2021	21.01.2021	20.02.2021
		28.02.2021	07.03.2021
		13.03.2021	24.03.2021
		29.03.2021	07.04.2021

Table 1 Streamer events above Northern Atlantic from January 2020 until March 2021 and related start and end dates. The right part shows calm periods.

Figure 1 shows the TO3 by TOPOMI/S5P integrated from November 3rd to November 5th 2020. Ozone-poor airmasses (blue) are located above the Northern Atlantic from 30°N to 70°N next to smaller scale ozone-poor airmasses above western North America and Central Asia. The TO3 concentration is disturbed by planetary waves along the latitudes, which lead to wave structures visible especially at the transition of blue to green colors. A large streamer event of ozone-poor airmasses is detected over the Northern Atlantic. A small streamer can be detected over western North America. There are also ozone-poor air masses above eastern

Europe. The temporal evolution shows, that the ozone-poor air masses above eastern Europe are due to a decaying streamer which evolved several days earlier. As planetary waves are more or less permanently disturbing the atmospheric ~~dynamic~~dynamics, especially smaller scale streamers can be detected almost every day. In this example, the streamer event above the Northern Atlantic is largest. Therefore, we consider this event for the further analysis.

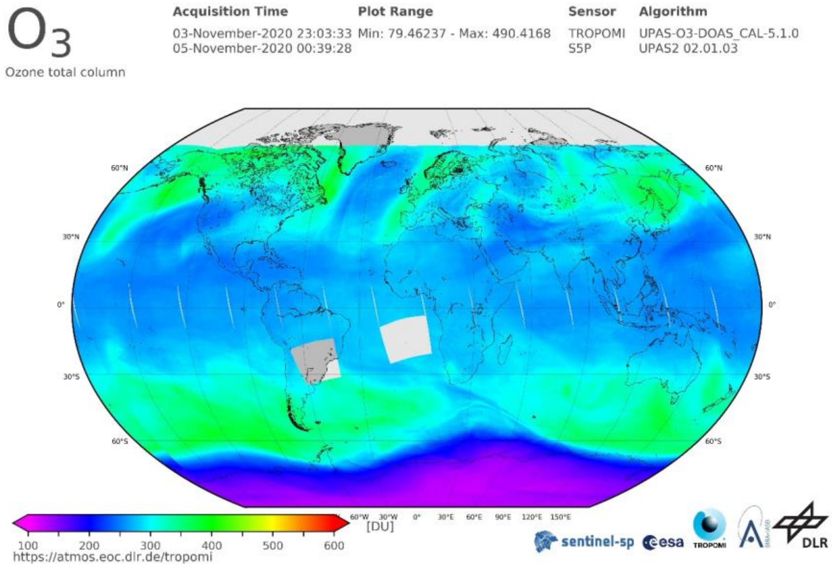

Fig. 1. TO3 by TROPOMI/S5P from November 3rd to November 5th 2020 shows ozone poor airmasses above the Northern Atlantic as an example of a streamer event for the further analysis. Colors (from violet to red) indicate the total ozone column concentrations (from low to high) in Dobson Units. Source: DLR, CC-BY 3.0

Figure 2 shows the TO3 by TOPOMI/S5P from February 11th to February 13th 2020. The event is characterized by a strong meridional gradient from the equatorial to polar region on the Northern Hemisphere with almost no longitudinal variation. ~~We assume, that planetary waves~~ Therefore, we consider this event for the further analysis.

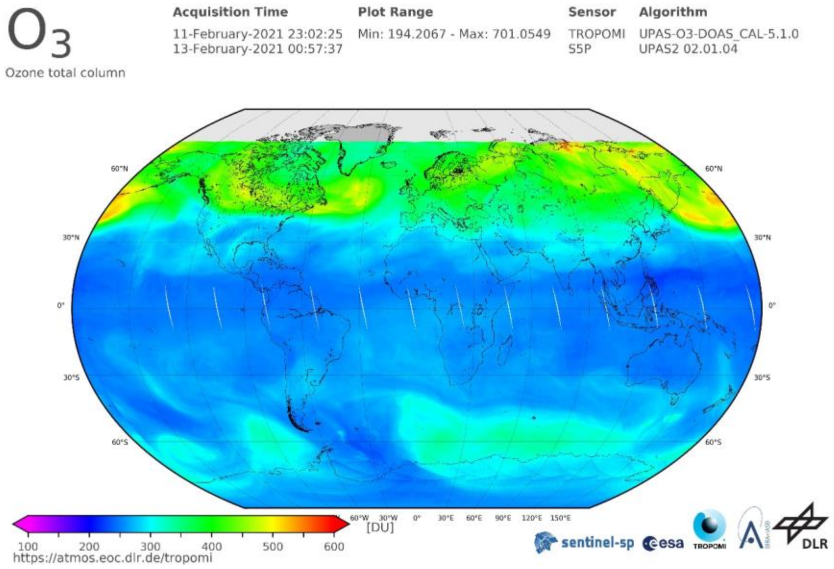

Fig. 2. TO3 by TROPOMI/S5P from February 11th to February 13th 2020 as an example of calm atmospheric dynamics. A clear meridional gradient of ozone can be observed on the Northern Hemisphere without large-scale wave structures. Colors (from violet to red) indicate the total ozone column concentrations (from low to high) in Dobson Units. Source: DLR, CC-BY 3.0

Two stations of the Czech microbarograph network~~,~~ (Bondar et al., 2022) are involved in the study – the large aperture array WBCI (50.25°N 12.44°E) and the small aperture array PVCI (50.52°N 14.57°E). To study propagation of GW and long-period infrasound (from acoustic cut-off up to about 2.5 s) pressure recordings at WBCI are utilized. Four sensors of the WBCI array are arranged in a tetragon. The inter-element distances of 4 – 10 km define an optimum performance of the array in the infrasound frequency range from the acoustic cut-off frequency of 0.0033 to 0.0068 Hz (Garcès, 2013). The WBCI array with its large inter-element distances has a unique configuration compared to the arrays of the International Monitoring System of the Comperehensive Nuclear Test Ban Treaty Organisation intended for infrasound monitoring in the frequency band of 0.02 – 4 Hz (Marty, 2019). Each array element at WBCI is equipped with an absolute microbarometer of the type Paroscientific 6000-16B-IS with parts-per-billion resolution. ~~Sampling frequency is 50 Hz and a~~A GPS receiver is used for time stamping. ~~In~~Data are stored with a sampling rate of 50 Hz. For infrasound ~~studies,~~monitoring, WBCI data are resampled at 10 Hz sampling rate~~ are used~~. To detect and analyze GW, 1-min mean values of the absolute pressure data are used.

The small aperture array PVCI provides optimal precision of detections in the frequency range of 0.14 – 3.4 Hz (Garcès, 2013). Three sensors are arranged in an equilateral triangle; the array aperture is 200 m. The differential sensors of the type Infrasound Gage ISGM03 manufactured by the Scientific and Technical Centre give a flat response in the frequency range of 0.02 – 4 Hz. A GPS receiver is used for time stamping. The data are stored with a sampling frequency of 25 Hz~~; a GPS receiver is used for time stamping~~. This sampling rate is also used in regular processing of infrasound detections at PVCI.

Infrasound detections ~~at WBCI and at PVCI~~ are processed using the Progressive Multi-Channel Correlation (PMCC) detection algorithm (Cansi, 1995; Le Pichon and Cansi, 2003). PMCC analyses pressure recordings from an infrasound array and looks for coherent signals in overlapping time windows in several frequency bands (Le Pichon and Cansi, 2003). An elementary detection with the PMCC, or the detection pixel is declared in the time-frequency window, when signal correlation and consistency criteria are met. Detection pixels are grouped into the detection families based on similar time, frequency, azimuth of signal arrival, and signal trace velocity (Brachet et al., 2010). The arrival parameters of the detected infrasound are stored in the detection bulletins. The parameters of interest for the present study include time of arrival, azimuth of arrival, trace velocity, frequency, and amplitude. The PMCC configuration is set on an individual basis and is optimized for the given array (Brachet et al., 2010; Garcès, 2013; Szuberla et al., 2004~~). From the resulting PMCC detection bulletins infrasound arrival parameters of interest are extracted and used in the statistical analysis: time of arrival, root-mean-square (RMS) amplitude, azimuth of arrival, and mean frequency.~~); main parameters of the PMCC settings for the arrays PVCI and WBCI are given in Table 2.

Station	PVCI	WBCI
Detection range	0.09-7 Hz	0.0033-0.4 Hz
Length of the detection window; frequency dependent	412.84-6.44 s	2555-118 s
Adjacent windows overlap	95 %	90 %
Consistency	0.1 s	3 s
Azimuth tolerance for families forming	10°	3°
Family size	10-50 pixels	15-50 pixels

Frequency range analysed in the study of streamer events	0.09-0.4 Hz	0.0033-0.4 Hz

Table 2. Main parameters of PMCC configurations for the arrays PVCI and WBCI.

Infrasound propagation is modelled with the InfraGA/GeoAc raytracing tools (Blom and Waxler, 2012; Blom, 2019). InfraGA/GeoAc provides simulations of signal propagation from a point source; propagation through the range dependent atmosphere is modelled for the present study. Atmospheric characteristics are obtained from the G2S model (Drob et al. 2003). Verticals profiles of temperature, zonal and meridional winds, density and pressure are an input for the InfraGA/GeoAc. The grid of profiles covers the area from 45° to 65°N and from 30°W to 22.5°E; latitudinal step is 5° and longitudinal step is 7.5°. The location of the signal sources is estimated regarding atmospheric circulation at the tropopause and in lower stratosphere above the studied region.

Propagation of GW in the thermosphere/ionosphere is studied using the multi-point and multi-frequency continuous Doppler sounding system located in Czechia. Its advantage is a high time resolution (around 10 s) compared with ionospheric sounders (ionosondes) that measure the profile of electron densities in the ionosphere. ~~The continuous Doppler sounding is based on the measurement of Doppler frequency shift experienced by radio waves that reflect from the ionosphere.~~The frequency shift is due to the motion and electron density changes in the ionospheric plasma, caused for example by interaction with atmospheric waves propagating in the neutral atmosphere, with which the ionosphere (above ~ 80 km) merges. The sounding radio signal reflects at the height, where its frequency matches the so called local plasma frequency, which is determined by the local electron density. Therefore, the reflection height changes during the day and depends on the sounding frequency. Significant Doppler shifts, usable for analysis, are obtained if the signal reflects from the so called F2 layer (approximately 200 – 300 km). Several sounding frequencies are used in Czechia. The 3.59 MHz sounding was mostly effective at night, while the 4.65 MHz sounding provided good daytime data during the period analyzed. The propagation characteristics of GWs are calculated from the time delays between signals observed at the respective sounding paths (~~transmitter-receiver pairs).~~reflection points for each transmitter-receiver pairs) assuming that the reflection points are in the midpoints between each transmitter and receiver. A 60 or 90 min long time interval is usually used to calculate the velocities and azimuth of the observed waves. The methods are in detail described by Chum and Podolska (2018). The two-dimensional (2-D) version (propagation analysis in horizontal plane only) is anticipated for most of the studies, since a 3-D analysis requires simultaneous observation and signal correlation at different frequencies, which is often not the case, especially during solar minimum. Results of statistical investigation have been recently published (Chum et al., 2021). Identical methods of propagation analysis have been applied to investigate propagation of GWs in the troposphere based on data from large-aperture array WBCI (here the time delays are related to the locations of individual microbarometers). All analyses will be done with respect to the streamer events and calm periods shown in Table 1.

All analysis will be done with respect to streamer events the occurrence of which is shown in Table 1. We analyze winter period from 6 February 2020 to 7 April 2021. Calm periods can be found also in Table 1.

3) Results

3.1 Infrasound observations at ground stations WBCI and PVCI during streamer events 2020-2021

As in detail explained in the introduction, we investigate whether ground infrasound measurements can serve as a quick indicator of streamer events. Therefore, we compare infrasound detections during streamers with observations on calm days. Distinct differences are searched for, that can be revealed in routine processing of data from a **microbarograph** array. At first, we make a visual comparison of 2-D histograms of infrasound arrival parameters. Then mean values of two data sets – streamer events**arrays WBCI and PVCI in November 2020** **and** calm days – are compared; a two-choice hypothesis test using the central limit theorem is applied at the significance level $\alpha = 0.05$. **in March 2021**

$$u = \frac{\bar{x} - \bar{y}}{\sqrt{\frac{s_x^2}{n_x} + \frac{s_y^2}{n_y}}}$$

Where u is the test criterion, $\bar{x}$ and $\bar{y}$ are the means of the first and second data set, s_x^2 and s_y^2 are the variances, and n_x and n_y are the numbers of elements in the first and second data set, respectively. A normal distribution of u is expected when the mean values are equal.

3.1.1 Observations at WBCI during streamer events 2020-2021

Wave activity in the infrasound frequency range of 0.0033-0.4 Hz wasis investigated. The upper limit of the analysed band was set so that it includes microbaroms, although the combining observations at stations WBCI and PVCI. Infrasound detections at WBCI are processed in the frequency band of 0.0033 – 0.4 Hz. The operational range of the array was thusis extended towards higher frequencies compared with the above the upper limit of the optimum array range (0.0033 – 0.; the degraded performance of WBCI at frequencies higher than 0.0068 Hz shall be considered. The upper limit of the analysed band is intentionally set to 0.4 Hz to cover microbaroms. PVCI detections are analysed in the frequency range of 0.09 – 0.4 Hz. The band partly overlaps with the detection range of the WBCI array and at frequencies of 0.12 – 0.35 Hz it is dominated by microbaroms (e.g., Campus and Christie, 2010).) (Garcès, 2013). Unlike WBCI, PVCI provides an optimal performance in the microbarom band.

Microbaroms are infrasound signals generated by a non-linear interaction of ocean waves travelling in opposite directions. MicrobaromMicrobaroms form a wide peak around 0.2 Hz in infrasound spectrum; their frequency corresponds to twice the frequency of sea waves. Microbaroms form a wide spectral peak around 0.2 Hz. A powerful source of microbaroms is located in the North Atlantic and the signals are regularly detected by European infrasound stations (Hupe et al., 20182019). The detection capability of microbaroms from the North Atlantic is high particularly high from October to March when the source becomes stronger due to stormy weather above the ocean and signal propagation to the East from the source is supported by the stratospheric waveguide (Landès et al., 2012). From the global point of view, microbaroms are permanently present in recordings of infrasound stations worldwide.

A class A streamer event occurred on 3rd – 7th November 2020. WBCI recorded infrasound in a few sparse intervals on 3rd November at 00-09 UTC, on 5th – 6th November at 19-05 UTC, and on 7th November at 16-24 UTC from back-azimuths of 250°-305° and later from back-azimuths of 305°-340° (Figure 3). The signal frequencies on 5th – 6th November differed from those on 3rd November and 7th November: frequencies of ~0.04 Hz were observed on 5th – 6th November while on 3rd and 7th November they were around 0.2 Hz.

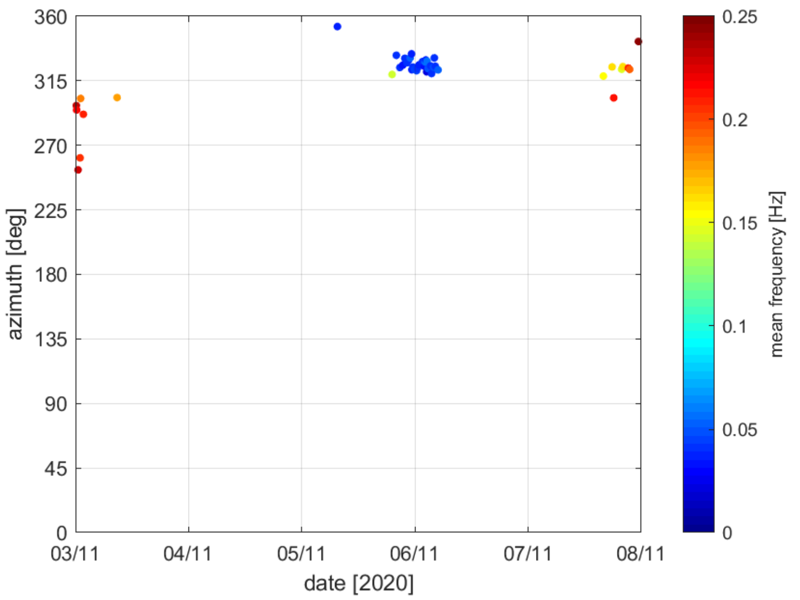

~~**Figure 3**~~We analyse infrasound observations from 3^{rd} to 25^{th} November 2020 and from 28^{th} February to 25^{th} March 2021. In these time intervals adjacent streamers and calm periods occurred (Table 1). Streamers and the calm period in the November 2020 time window are evaluated separately from those in the March 2021 time window to avoid seasonal influences. While a well-developed stratospheric waveguide can be expected in November, its efficiency can decrease in March due to coming seasonal reversal of stratospheric winds.

3.1.1 Infrasound observations from 3^{rd} to 25^{th} November 2020

Two streamer events developed in November 2020. The first streamer occurred from 3^{rd} to 7^{th} November and the second one from 21^{st} to 25^{th} November. The streamers were separated by a calm period from 9^{th} to 15^{th} November.

WBCI provides rather sparse detections during both streamer events and only two detection families are obtained during the seven-day calm period (Figure 3). The signal frequencies near 0.2 Hz and back-azimuths of 290° – 350° indicate that the observed signals are likely microbaroms from the North Atlantic. A decrease of the signal frequency is observed during the first streamer event. On 5^{th} – 6^{th} November from 20 to 05 UTC, the mean frequency of the north-west arrivals drops down to 0.04 Hz. Changing signal frequencies do not occur during the second streamer from 21st to 25th November.

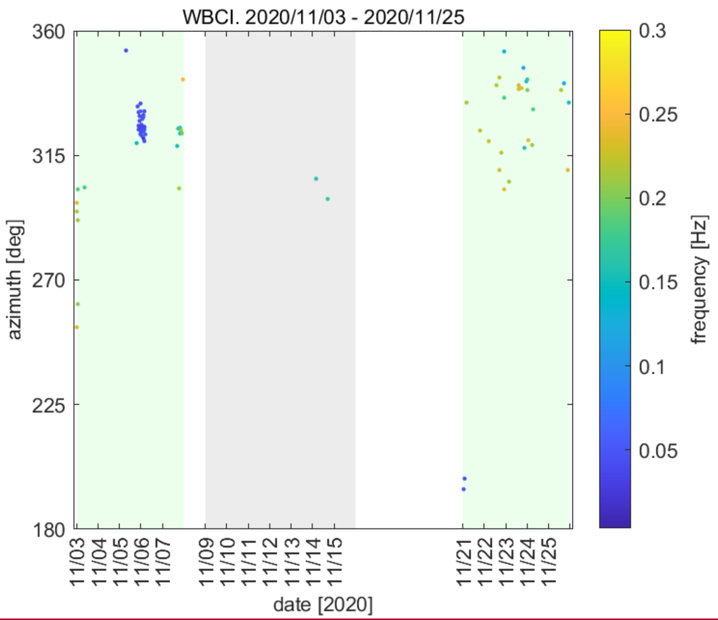

Fig. 3. Infrasound observations at WBCI on 3rd - ~~7th November 2020.~~25th November 2020. Azimuth of signal arrivals is shown; the colorbar refers to the mean frequency of the detection family. One circle in the plot represents one detection family. Green background marks the streamer events, grey background marks the calm period.

PVCI detects arrivals from the north-west as well (Figure 4). Fluctuating signal amplitudes are observed. Values around 0.02 Pa occur on 3 November. From 4th November, 18 UTC to 7th November, 22:30 UTC, the signals are of amplitudes around 0.089 Pa. The amplitudes decrease to the values around 0.046 Pa during the consequent quiet period and further to 0.024 Pa during the streamer on 21st – 25th November. Trace velocities are similar during streamers and quiet periods. The velocities fluctuate between 0.335 and 0.494 km·s^{-1}; no significant signatures of the streamers are identified in the signal trace velocity.

The observations at WBCI and PVCI from 3rd to 25th November 2020 can be summarized as follows. During the streamer event, the decrease in signal frequency is observed at

WBCI. At PVCI, the increased signal amplitudes occur. Signal trace velocities seem uninfluenced by the streamers.

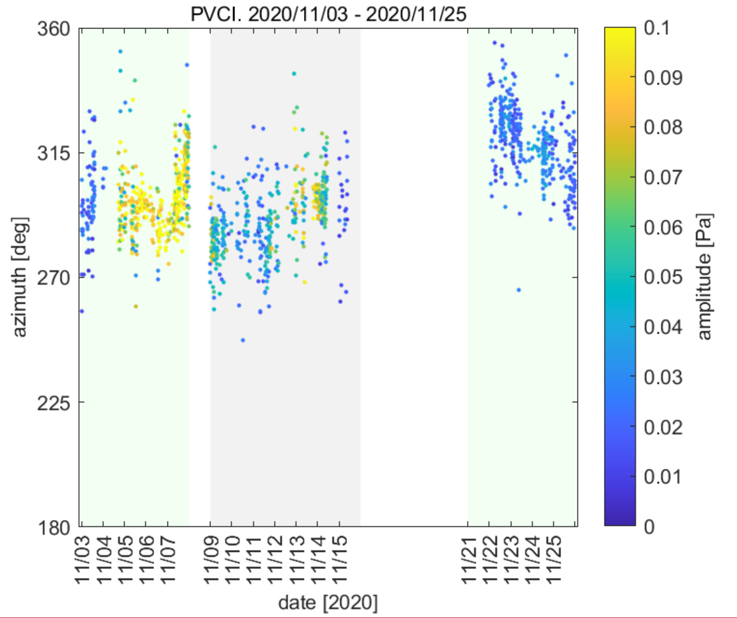

Fig.4. Infrasound observations at PVCI on 3rd - 25th November 2020. Azimuth of signal arrival is shown; the colorbar refers to the mean frequency of the detection family A detection family is a group of primary PMCC detections-so called detection pixels- merged together based on similarity of arrival parameters carried by the pixels. One circle in the plot represents one detection familysignal amplitude. Green background marks the streamer events, grey background marks the calm period.

Infrasound detections were sparse also in the other studied streamer events and calm periods. The streamer events occurred on 35 days between February 2020 and April 2021, 247 infrasound detections were obtained. Within the same time window, 867 infrasound detections on 153 calm days were found. To avoid possible distortion of the results due to a single extreme value in a small dataset, we did not evaluate the infrasound arrival parameters during the respective streamers, but we grouped the observation in an overall data set and compared its mean values against the reference group of all calm days within the studied time period. We cannot reject that signal amplitudes are same during streamer events and on calm days at the significance level $\alpha = 0.05$. Mean signal frequency is higher in the group of days with streamer events at the significance level $\alpha = 0.05$, or with 95% reliability. Details are presented in **Table 2.** and visually can be seen on Figure 4 and 5. Notice that contrary to the result for the overall data sets, the signal frequencies transiently decreased from ~0.2 Hz to ~0.04 Hz during the class A streamer on 3rd—7th November 2020. Besides possible influences of changed dynamics in the lower/middle atmosphere on infrasound propagation, modification of the infrasound source shall be considered on 3rd—7th November 2020. There was a large pressure gradient above the North Atlantic (earth.nulschool.net, www2.wetter3.de, www.ventusky.com). The WAVEWATCHIII® wave-action model (The WAVEWATCHIII® Development Group, 2016) predicted an increase of significant height of combined wind waves and swell in the North Atlantic particularly on 5th—6th November 2020; the peak wave periods stayed in the interval from 10 to 15 s on 3rd—7th November 2020 (plots not shown here). To investigate properly the influence of source-related and signal-propagation factors on infrasound detections at WBCI during the streamer event, a complex study including infrasound source and propagation modeling is necessary. However, this is out of the scope of the present paper and it can be performed in a future dedicated study.

Tohle je adresa zdroje dat : WAVEWATCHIII data at https://polar.ncep.noaa.gov/waves/ensemble/download.shtml, accessed on 14 March 2023

Commented [t1]: Nevím, jaké budou od časopisu požadavky na citaci internetového zdroje, takže nechávám ve formě poznámky. A pak ve finální verzi musíme řádně citovat.

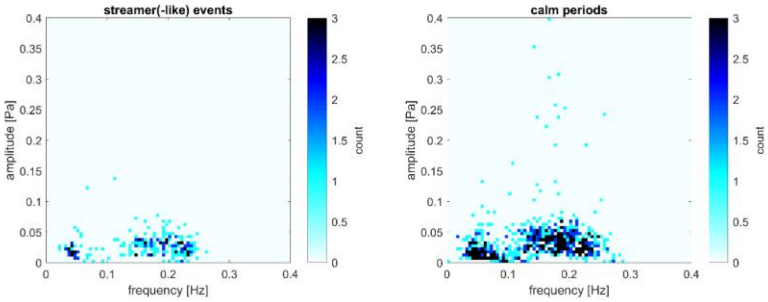

Figure 4 2D histogram frequency vs. amplitude of signals measured at WBCI. Left panel: summary of streamer events 2020-2021, right panel: calm period 2020-2021 as reference data. The colorbar shows number of detections in the respective frequency-amplitude bins.

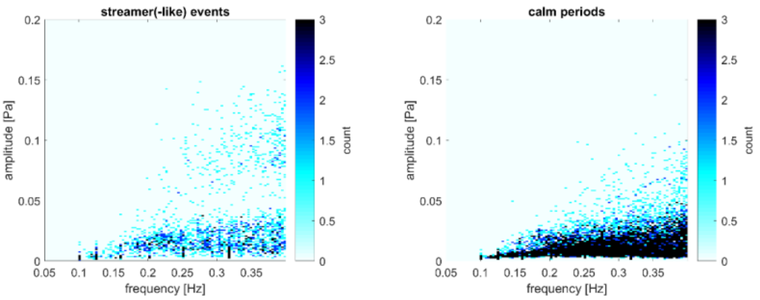

Figure 5 2D histogram frequency vs. amplitude of signals measured at PVCI. Left panel: summary of streamer events (3rd–7th November 2020, 21st–25th November 2020, and 9th–12th March 2021), right panel: calm periods as reference data (2nd–14th March 2020, 9th–15th November 2020, 18th–22nd December 2020, 1st–7th March 2021, and 14th–24th March 2021). The color bar shows number of detections in the respective frequency-amplitude bins

3.1.2 Observations at PVCI

The performance of the WBCI array at the upper limit of the frequency band of interest, the microbarom band can be degraded. Therefore, the PVCI array is included in the study the performance of which is optimal in the 0.12 – 0.35 Hz microbarom band.

Infrasound detections for selected streamer events were analysed: 3rd – 7th November 2020, 21st – 25th November 2020, and 9th – 12th March 2021 (Figure 6). PVCI data were not available for most of the streamer event periods on 6th – 10th February 2020 and on 23rd – 27th February 2021. We focused on streamer events that occurred in the season of winter stratospheric westerlies, which lasts usually from November to March (Le Pichon et al. 2012). In winter, infrasound stations largely detect sources located to the west from the station. Streamer events typically occur above Western Europe and adjacent regions of the North

Atlantic. Therefore, winter is the season, when Central European infrasound stations are able to detect signals arriving from or through the regions of streamer events. Observations during calm periods on 2nd—14th March 2020, 9th—15th November 2020, 18th—22nd December 2020, 1st—7th March 2021, and 14th—24th March 2021 were used as a reference data set.

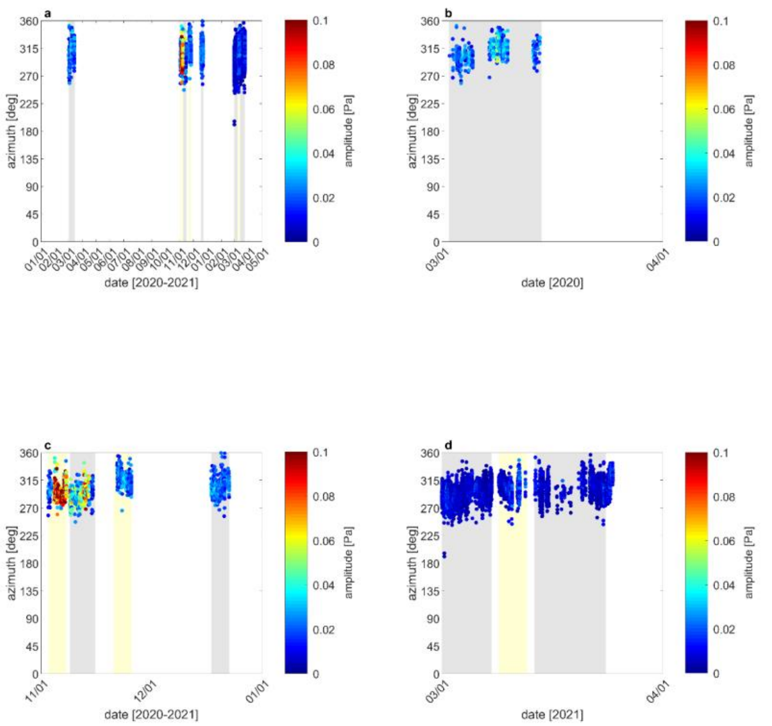

Figure 6 Infrasound detections at PVCI during streamer events (yellow fields) and calm periods (grey fields) in 2020 and 2021. Azimuth of signal arrival is shown; the color bar refers to the signal amplitude. Panel (a): overview plot of all analyzed periods; panels (b)-(d): zoom at March 2020, November-December 2020, and March 2021

Taking into account the mutual positions of PVCI and the region of typical occurrence of streamers, we analysed signals arriving from the back-azimuths of 180—360°. We focused on detections in the frequency range of 0.05 – 0.4 Hz. The band partly overlaps with the detection range of the WBCI array (0.0033 – 0.4 Hz) and at frequencies of 0.12 – 0.35 Hz it is dominated by microbaroms (e.g., Campus and Christie, 2010).

High sensitivity of the PVCI array in the microbarom frequency range enabled to compare the respective streamer events with the reference data separately. As we focus on signal analysis in a narrow frequency range (0.05 – 0.4 Hz), signal frequency during streamer events and its departures from calm-day values were not analyzed. Higher mean signal amplitude was proved on the significance level $\alpha = 0.05$, or with 95% reliability during the streamer events on 3rd – 7th November 2020 and 21st – 25th November 2020. It was not rejected that the signal amplitudes during streamer event on 9th – 12th March 2021 are same as on the calm days. Details can be found in Table 3. The highest difference of signal amplitudes compared to the set of calm days was found during the streamer on 3rd – 7th November 2020; mean signal amplitude of 0.013 Pa was obtained on the calm days, whereas on 3rd – 7th November the mean amplitude increased to 0.077 Pa. As discussed in section 3.2.1, the microbarom source in the North Atlantic was possibly intensified by a maritime storm that was in progress during the considered time interval.To approximate propagation of signals from a source located at the surface of the North Atlantic, the InfraGA/GeoAc tools are employed. Propagation of the 0.2 Hz signals is modelled on 6th November at 00 UTC. Three scenarios represent propagation conditions influenced by a streamer event. The fictitious point sources are located (1) at 55°N and 15°W, (2) at 55°N and 5°W, and (3) at 60°N and 0°longitude. The coordinates of the sources are estimated based on the position of the tropopause jet stream disturbance. Taking into account the mutual locations of the sources and the receiving arrays, eastward signal propagation is modelled. The azimuth limits are set to 0° and 180°, the azimuth step is 3°. Signal inclinations 2° – 45° are considered in 2° resolution. As a reference, signal propagation from a source at 55°N and 15°W is modelled on the calm day, 12th November at 00 UTC.

Stratospheric arrivals are expected by the model in Central Europe from the sources at the latitude of 55°N during the streamer event as well as on the calm day. Signal propagation through the thermospheric waveguide is possible from all the considered sources during the streamer event and on the calm day (Figures 5 – 8). The decrease of signal frequency observed at WBCI on 5th – 6th November from 20 to 05 UTC can indicate that thermospheric ducting transiently prevailed over the stratospheric waveguide.

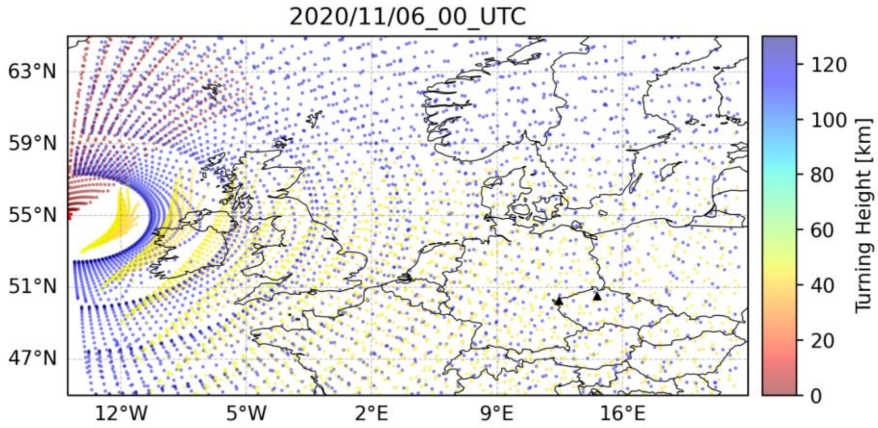

Fig.5. Model of infrasound propagation from a point source located at 55°N and 15°W (red asterisk) during the streamer event on 6th November 2020 at 00 UTC. Colobar refers to the turning heights of the signal. Red indicates signal propagation in the waveguide formed near the tropopause (altitudes around 10 km), arrivals through the stratospheric waveguide are in yellow (altitudes around 40-50 km) and arrivals through the thermospheric waveguide are in blue (altitudes above 100 km). Black triangles represent infrasound arrays WBCI (the left triangle) and PVCI (the right triangle).

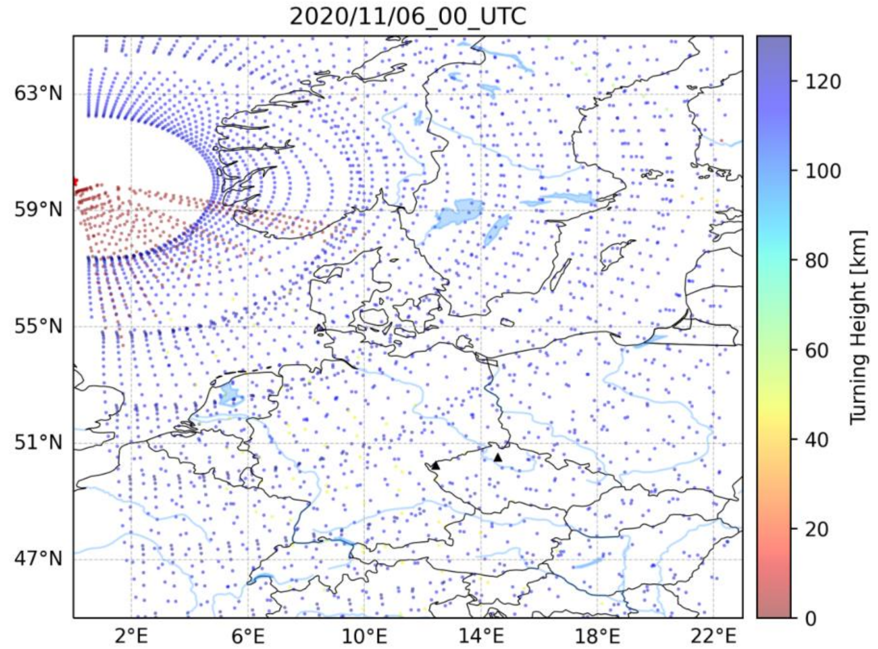

Fig.6. The same as Figure 5, but for the source located at 60°N 0°longitude. The stratospheric waveguide is not significantly involved in infrasound ducting to Central Europe.

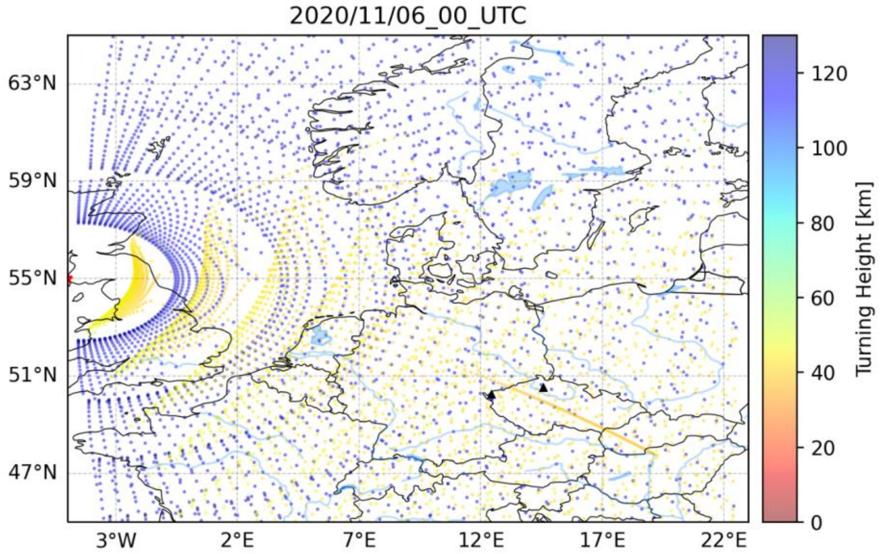

506

507 Fig.7. The same as Figure 5, but for the source located at 55°N 5°W. The tropospheric

508 waveguide does not influence propagation to the East of the source.

509

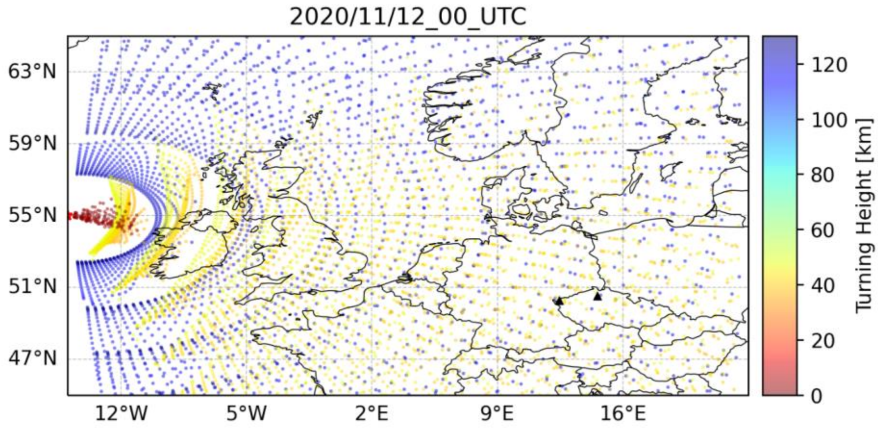

Fig.8. Model of infrasound propagation from a point source located at 55°N and 15°W (red asterisk) on the quiet day of 12th November 2020 at 00 UTC. The meaning of the symbols and colours is the same as in Figure 5.

It follows from Figures 5 – 7, that the effects of the streamer event occur in the limited regions close to the sources. Northward propagating signals from a source at 55°N and 15°W are guided by the northward jet-stream above the source location (Figure 5). Signals from the source at 60°N 0°longitude propagate in the opposite direction; southward waveguide at the tropopause is formed by the southward jet-stream near the west coast of southern Scandinavia (Figure 6). Tropospheric – tropopause ducting is not predicted for signals emitted by the source located between the northward and southward branch of the jet-stream wave (Figure 7). It follows from the InfraGA/GeoAc outputs that signal propagation from sources in the North Atlantic to Central Europe is not significantly modified by the streamer event on 6th November 2020 at 00 UTC.

Publicly available data – meteorological charts provided by Deutscher Wetterdienst and the WAVEWATCHIII® wave-action model (The WAVEWATCHIII® Development Group, 2016) indicate that there was a maritime storm in progress in the North Atlantic within the time window of the first streamer. The storm could cause intensification of the microbarom source and as a consequence, increased signal amplitudes were observed at PVCI on 4th – 7th November.

3.1.2 Infrasound observations from 28th February to 24th March 2021

A streamer event occurred from 9th to 12th March 2021 preceded and followed by calm periods from 28th February to 7th March and from 13th to 24th March, respectively.

Both WBCI and PVCI detect signals arriving from the north-west, from back-azimuths of 285° – 310°. An increase of signal trace velocities is observed in some of the detections at WBCI during the streamer event compared to calm periods (Figure 9). Trace velocities of 0.460 km/s and 0.380 km/s are observed from back-azimuths of 270° and 310° on 10th March at 00 – 06 UTC, respectively. It is by 0.05 – 0.13 km/s higher than on the calm days. Contrary, PVCI records a decrease in trace velocities on 10th March at 00 – 06 UTC (Figure 10). Trace velocities of 0.377 km/s are observed compared to 0.413 km/s and 0.395 km/s during the calm periods before and after the streamer, respectively. Differences between the streamer event and calm periods are not observed in signal amplitudes and frequencies. Mean signal frequencies remain around 0.2 Hz and amplitudes vary between 0.003 and 0.049 Pa without any trend.

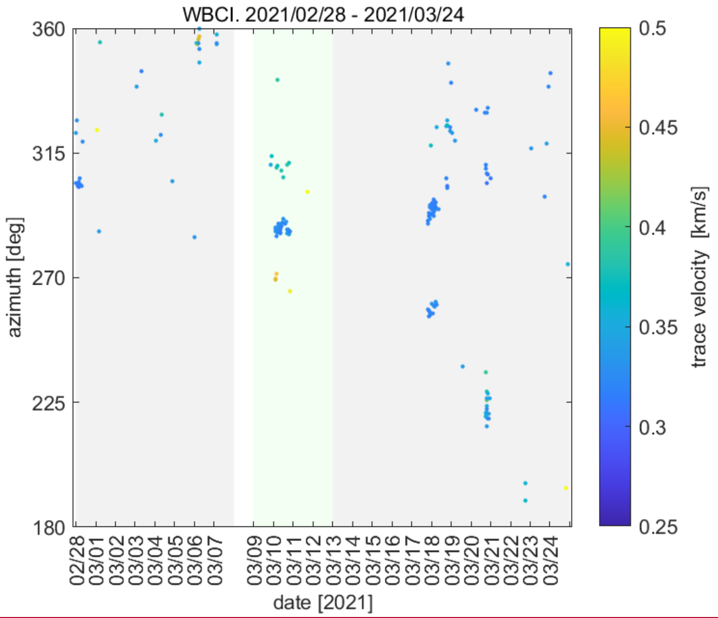

Fig.9. Infrasound observations at WBCI on 28th February – 24th March 2021. Azimuth of signal arrival is shown; the colorbar refers to the signal trace velocity. Green background marks the streamer event, grey background marks the calm periods.

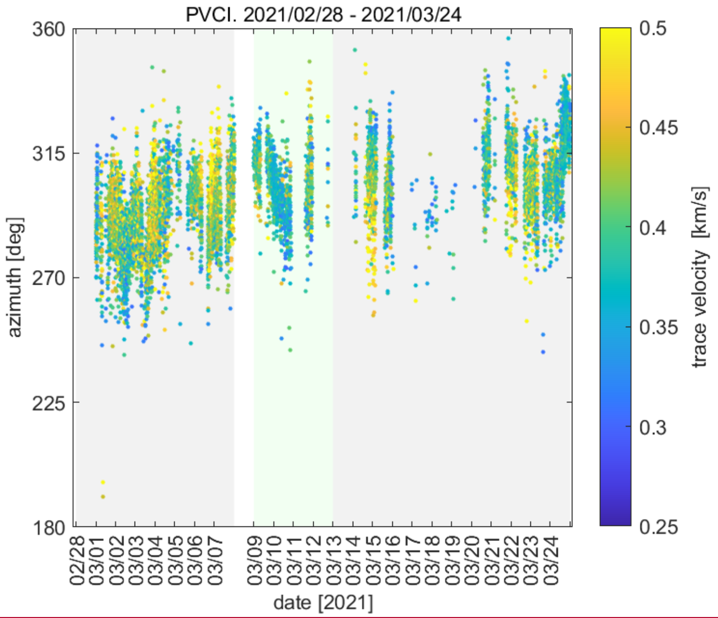

Fig.10. Infrasound observations at PVCI on 28th February – 24th March 2021. Azimuth of signal arrival is shown; the colorbar refers to the signal trace velocity. Green background marks the streamer event, grey background marks the calm periods.

The different trace velocities observed during the streamer event and during the calm periods can indicate modifications of the atmospheric waveguides. The theoretical relationship between the signal trace velocity and celerity presented by Lonzaga (2015) relates lower trace velocities to signals refracted at lower altitudes. The exact limits of the trace velocity for the given atmospheric waveguide depend on the current state of the atmosphere. The decrease of the trace velocities observed at PVCI can indicate transient signal propagation in the tropospheric waveguide. Increased trace velocities at WBCI can be explained as arrivals from the upper atmospheric regions. However, effects of spatial aliasing must also be taken into account at the WBCI detections, especially considering that the signal frequencies are around 0.2 Hz, well above the range of array optimum performance. The observed increase of trace velocities at WBCI can therefore be a processing bias rather than a consequence of signal refraction at higher altitudes.

Like in the November 2020 case, we employ the InfraGA/GeoAc tools to investigate infrasound propagation paths on 10th March at 03 UTC. Propagation of the 0.2 Hz signal is modelled. A source is located at 55°N 15°W; this scenario represents signal propagation from the central North Atlantic. The other source is located at 55°N 0°latitude representing propagation of microbaroms from the North Sea. Propagation in azimuths 0° – 180° of the source is studied. For both sources, InfraGA/GeoAc predicts eastward signal propagation in the stratospheric and thermospheric waveguides. The other eastward waveguide occurs near the tropopause, formed by the eastward to south-eastward jet-stream above the eastern North Atlantic and Western Europe at latitudes 50 – 60°N. Signals emitted by a source in the North Sea are expected to propagate also through this waveguide to Central Europe (Figure 11). Though the simulation of signal propagation from a point source is an approximation of the real situation – microbaroms are emitted by a source that is considered planar, the model results suggest that the fluctuations of microbarom trace velocity observed at PVCI on 10th March 2021 can be influenced by the tropospheric waveguide. Tropospheric waveguides in general are considered less stable compared to the waveguides in the middle and upper atmosphere (Drob et al., 2003).

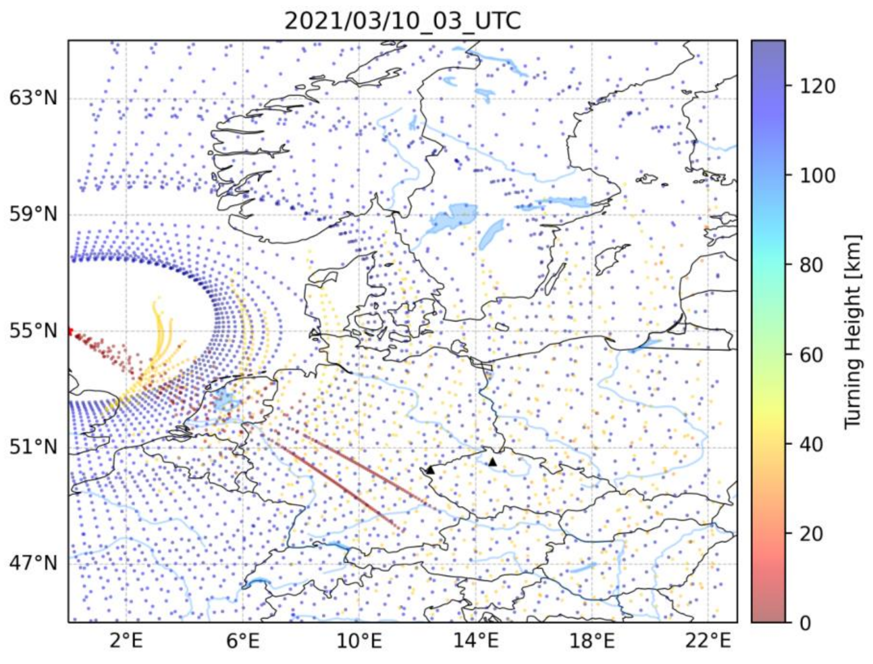

Fig.11 Model of infrasound propagation from a point source located at 55°N and 0°longitude (red asterisk) on 10th March 2021 at 03 UTC. The waveguide near the tropopause is expected to influence infrasound propagation to Central Europe.

3.2 Results and discussion of gravity waves in the troposphere and ionosphere

3.2.1 Investigation of GWs measured on the ground by WBCI array of micro-barometers.

. Figure 712 shows the RMS amplitudes of pressure fluctuations- in the period range 5-60 min recorded from November 1 to November 9, 2020. This interval covers a distinct streamer event that occurred from November 3 to November 7. The results of propagation analysis are shown in Figure 813, which- displays the phase velocities and azimuths of GWs. Only results that satisfied the criterion (dv/v <0.0.5) and (dAZ<10°) and (p_{RMS}>0.02 Pa) are presented, where dv/v, dAZ, p_{RMS} are the relative uncertainty of GW phase velocity, uncertainty of azimuth and root mean square value of pressure fluctuations in the analysed time interval. Figure 813 demonstrates that there is a tendency for higher phase velocities and occurrence of different azimuths during the streamer event. Therefore, it is useful to compare the GW characteristics during streamer events and calm conditions.

Figure 914 shows histograms obtained by a statistical analysis. The RMS amplitudes of pressure fluctuations in the period range 5- – 60 min, phase velocities and azimuths were investigated separately for calm conditions (upper plots) and for streamer and streamer-like events listed in Table 1 (bottom plots).) with a 1-hour time resolution. The solid vertical lines mark lower (Q1) and upper (Q3) quartiles. The dashed vertical lines depict boundaries for large (Q3+1.5·(Q3-Q1)) and extreme (Q3+3·(Q3-Q1)) values. A difference between histograms for RMS pressure fluctuations and azimuths obtained for calm and disturbed conditions is obvious. A minor difference is also observed for phase velocities.

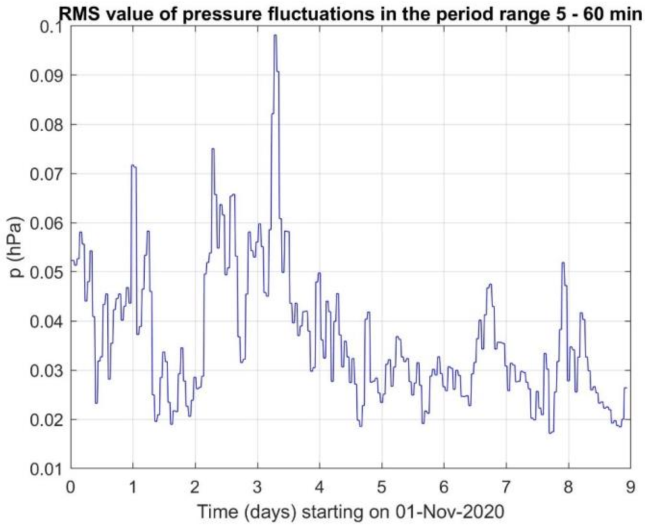

Figure ~~7~~12 Amplitude of GWs recorded by WBCI from 2020-11-01 to 2020-11-09

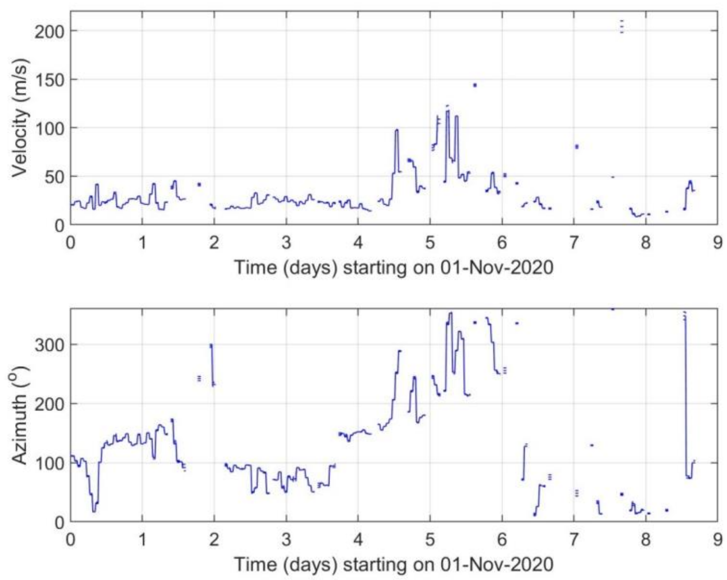

Figure ~~8~~13 Propagation velocity and azimuth of GWs recorded by WBCI from 2020-11-01 to 2020-11-09

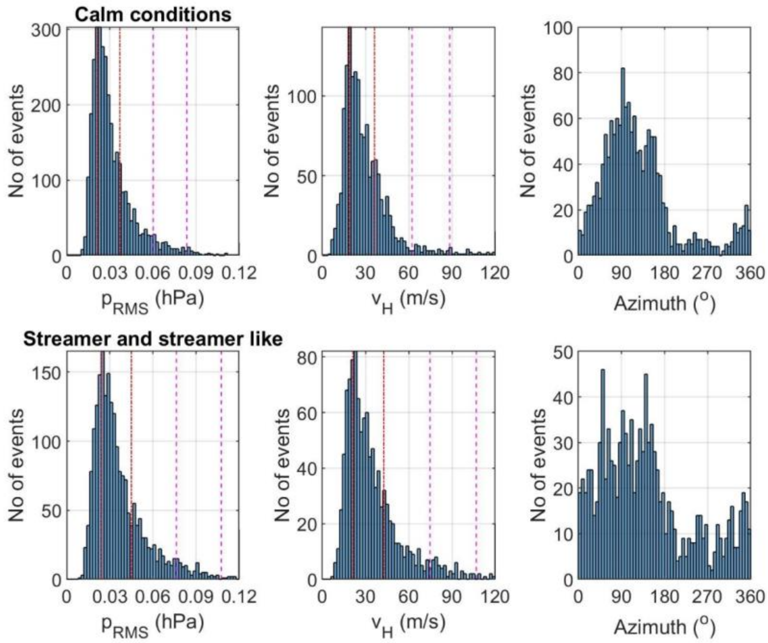

Figure ~~9~~14 GW characteristics (RMS of pressure fluctuations, phase velocity and azimuth) for calm periods (upper plots) and streamer and streamer like events (bottom plots) for 2020 and winter 2021. The red vertical lines mark lower (Q1) and upper (Q3) quartiles. The dashed magenta vertical lines depict boundaries for large (Q3+1.5·(Q3-Q1)) and extreme (Q3+3·(Q3-Q1)) values.

3.2.2 Investigation of GWs measured in the ionosphere by continuous Doppler sounding system (CDS)

The 2D propagation analysis of GWs was performed using the 2D versions of methods mentioned in Section 2 and in detail described by Chum and Podolská (2018). ~~The~~As discussed in Section 2 and by (Chum et al., 2021), the 2D propagation analysis makes it possible to analyze much larger number of time intervals than the 3D analysis ~~(Chum et al., 2021).~~. The propagation analysis obtained for the interval from 1st November to 9th November 2020, which covers the significant streamer event that occurred from 3rd November 2020 to 7th November 2020, is presented in Figure ~~10~~15. Only results that satisfied the ~~criterion~~criteria (dv/v <0.2) and (dAZ<20°) and (f_{DRMS}>0.05 Hz) and (C_{max}<0.5) are presented, where dv/v is the relative uncertainty of GW phase velocity, dAZ is the azimuth uncertainty, f_{DRMS} is the root mean square of the Doppler shift in the analysed time interval and C_{max} is the maximum in the normalized energy map for the best beam (slowness) search; C_{max} is 1 for identical signals (Chum and Podolská, 2018). It is considered that signals are not sufficiently correlated (coherent) for reliable propagation analysis if C_{max} < 0.5 (Chum et al., 2021). The velocities and azimuth obtained by observation at 3.59 MHz are in red, whereas the values based on measurements at 4.65 MHz are in blue. Obviously, the observations at 3.59 MHz mostly ~~corresponds~~correspond to the nighttime, whereas observations at 4.65 MHz were mostly made during the daytime. The 4.65 MHz signal did not reflect from the ionosphere (escaped to the outer space) at night due to the low critical frequency of the ionosphere. On the other hand, the 3.59 MHz signal mostly reflected during the day from the ionospheric E layer and the Doppler shift was negligible, difficult to analyse.The GWs usually propagated roughly poleward at night and roughly equatorward during the daytime. This is fully consistent with the statistical investigation (Chum et al., 2021) ~~who~~which showed that propagation directions of GWs in the ionosphere exhibit diurnal and seasonal behaviour and are mainly controlled by the neutral winds in the thermosphere.

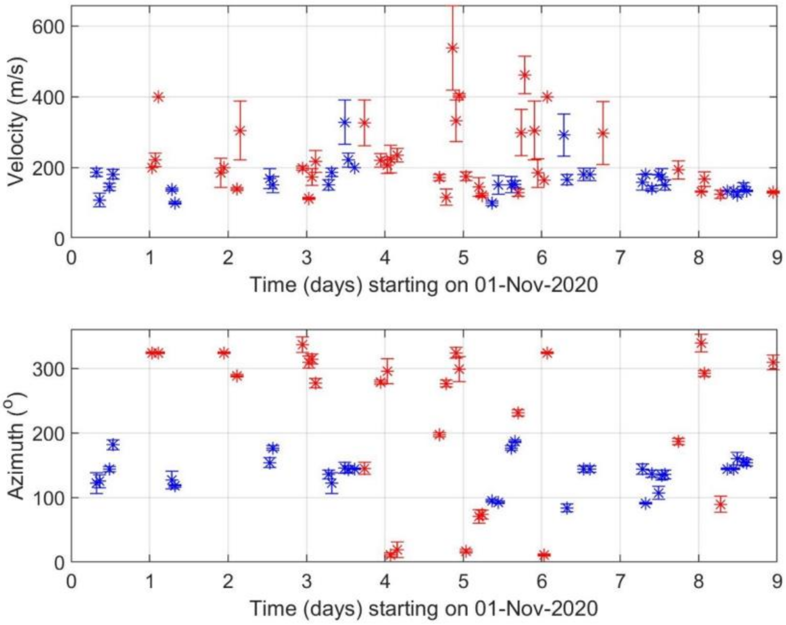

Figure ~~10~~15 Propagation velocity and azimuth of GWs in the ionosphere obtained using CDS measurements from 2020-11-01 to 2020-11-09. The velocities and azimuth obtained by observation at 3.59 MHz are by red, whereas the values based on measurements at 4.65 MHz are by blue.

Based on the analysis of the GW observed in the ionosphere during the streamer event and on the previous statistical analysis, we conclude that no obvious signature related to streamer event was observed for the propagation of GW the ionosphere.

It should be also mentioned that the phase velocities of GW measured on the ground (Figure 8) and at heights around 200 km in the ionosphere differ. There are several reasons for that. First, the observed horizontal phase velocities depend on the elevation angle of GW propagation and on the ambient temperature as follows from the dispersion relation (the temperature enters the dispersion relation via the buoyancy frequency and the scale height). The temperature in the ionosphere/thermosphere is several times higher than in the troposphere. The elevation angles might change during the upward propagation of GWs, depending on the wind and temperature profile. Second, GWs propagate with a tilt, not vertically upward. It is therefore highly probable that the sources of the GWs observed in the troposphere and ionosphere are different. Moreover, GW can break during their propagation upward and secondary gravity waves might be observed in the ionosphere.

4) Conclusion and discussion

The focus of this study was to test independent types of observations like Doppler sounding and ~~infrasound detections~~microbarograph measurements for an analysis of GW behavior during streamer events, which are strongly connected with PW or GW and the large scale mass transport of ozone and that is why it can be very interesting for studies of atmospheric dynamics.

The other aim of the study was to find phenomena in infrasound arrival parameters that could serve as a quick indicator of streamers and that could be identified ~~in~~during the routine processing of infrasound detections. ~~Simple visual comparison~~Infrasound observations at two Central European stations PVCI and WBCI were studied; signal propagation through a range dependent atmosphere was modelled using the InfraGA/GeoAc tools. In November 2020 and in March 2021, the dynamics of ~~infrasound arrivals during~~the tropopause – lower stratosphere region was influenced by streamer events~~ and on calm days (Figures 4 – 6) did not reveal significant and easy-to-identify deviations of the arrival parameters – the azimuth of arrival, RMS signal amplitude and ~~. During the streamer in November 2020, a transient decrease of signal frequency~~. The statistical analysis showed larger~~ was observed at WBCI; at PVCI signal amplitudes ~~at PVCI during two of three analysed streamers (Table 3). At WBCI~~varied. Streamer-related signatures were observed in trace velocities at neither of the stations. Contrary in March 2021, fluctuations of signal trace velocities occurred; the other signal arrival parameters were not influenced by the streamer. Amplitude fluctuations at PVCI in November 2020 were likely related to a variable intensity of the microbarom source caused by a maritime storm. The variations of trace velocities in March 2021, particularly at PVCI can be attributed to the waveguide which developed at the tropopause and which influenced signals propagating from the North Sea to Central Europe. In November 2020, signal propagation from the North Atlantic to Central Europe was not modified by the streamer. Signal propagation in the stratospheric and thermospheric waveguide was expected during the streamer event; similar propagation conditions occurred on the calm day. Since both waveguides were involved in infrasound ducting, it was ~~not rejected~~possible that ~~signal amplitudes are same during streamer events and on calm days (Table 2). Higher ~~WBCI transiently detected signals travelling in the thermospheric waveguide and as a consequence decrease of signal frequencies ~~were proved at WBCI in the streamer events data set than in the calm days data set. Yet, during the class A streamer event on 3rd – 7th November 2020, a transient decrease of the frequency of detected signal was recorded at WBCI. Based on these results, infrasound measurement at a single infrasound station cannot be recommended as a reliable sole indicator of streamers.~~ was observed.

~~Streamer events are limited in time and space. The observations of signatures of a streamer at an infrasound array can depend on the mutual positions of the source, the streamer region, and the observer. It is therefore suggested to analyse infrasound arrival parameters at a dense network of infrasound arrays that covers various directions and distances from the streamer region in order to reveal possible streamer event indicators. To explain properly the influence of streamers on infrasound propagation a dedicated 3D model study of infrasound propagation can be recommended. Infrasound sources in the present study were not well defined in terms of location, time, and intensity. Taking into account the aim of the present study – identification of an easy accessible and quick indicator of streamers in infrasound measurements, our results show some limitation but on the other hand it will be to benefit of future studies, if sources of the analyzed signals are better known and more events will be used for statistics.~~

Streamer events are dynamical phenomena. Their exact occurrence location as well as their impact on the tropopause – lower stratosphere region differs from event to event. It is therefore tricky to identify typical signatures of streamers in infrasound measurements that could serve as a reliable indicator of streamers.

Supplementary ground-based measurements of GW using the WBCI array in the troposphere showed that GW propagation azimuths were more random during streamer and streamer-like events compared to those observed during calm conditions. At the same time, larger GW amplitudes were observed in the troposphere during streamer and streamer-like events than under quiescent conditions. On the other hand, the GW propagation characteristics observed in the ionosphere by CDS during streamer events did not differ from those expected for the given time period, based on previous statistical studies (Chum et al., 2021).

~~More streamer events would need to be analysed to verify these preliminary results based on the limited number of events.~~

The results therefore indicate that streamers in the stratosphere might lead to changes in wave propagation in the troposphere. The impact on the ionosphere was not confirmed, but cannot be excluded due to spare and localized observations of GW activity. In general, to validate the preliminary results obtained in this study, a denser measurement network and more streamer events need to be analyzed.

Data availability:

ozone column measurements (TO3) which are available as a service by DLR at https://atmos.eoc.dlr.de/

Ground to space model vertical atmospheric profiles were obtained at https://g2s.ncpa.olemiss.edu/; accessed on 27 January – 4 February 2024

The WAVEWATCHIII® wave-action model data were accessed via ftp at polar.ncep.noaa.gov/waves/JCOMM/2020 on 13-14 March 2023.

The Deutscher Wetterdienst synoptic charts were accessed at https://www2.wetter3.de/archiv_dwd_dt.html on 3 February 2024.

Author contributions

MK and LK create the idea of manuscript; JCh, MK, TS, LK, and KP suggest the datasets and methods; TS, JCh, LK, KP and FT analyzed the data; MK wrote the manuscript draft; JCh, TS, LK and KP reviewed and edited the manuscript.

Competing interests

The authors declare that they have no conflict of interest.

Acknowledgement

The DTK-GPMCC software was kindly provided by Commissariat à l’énergie atomique et aux énergies alternatives, Centre DAM-Île-de-France, Département Analyse, Surveillance, Environnement, Bruyères-le-Châtel, F91297 Arpajon, France.

The authors are grateful to Dr. Phil Blom and Los Alamos National Laboratory for opening the InfraGA/GeoAc tools to the public.

Financial support: This study is supported by LISA project- Lidar measurements to Identify Streamers and analyze Atmospheric waves, AEOLUS-INNOVATION, Contract No. 4000133567/20/I-BG

Streamer events		**Calm periods**	
From	**To**	**From**	**To**
06.02.2020	10.02.2020	02.03.2020	08.03.2020
31.08.2020	03.09.2020	09.03.2020	14.03.2020
05.09.2020	11.09.2020	28.03.2020	10.04.2020
03.11.2020	07.11.2020	19.04.2020	27.05.2020
21.11.2020	25.11.2020	9.11.2020	15.11.2020
23.02.2021	27.02.2021	12.12.2020	22.12.2020
09.03.2021	12.03.2021	30.12.2020	06.01.2021
		21.01.2021	20.02.2021
		28.02.2021	07.03.2021
		13.03.2021	24.03.2021
		29.03.2021	07.04.2021

Table 1 Streamer events above Northern Atlantic from January 2020 until March 2021 and related start and end dates. The right part shows calm periods.

	mean	variance	number of detections
Frequency [Hz], calm days	0.147	0.005	867

Frequency [Hz], streamer events	0.160	0.005	247
RMS amplitude [Pa], calm days	0.043	0.019	867
RMS amplitude [Pa], streamer events	0.039	0.012	247

Table 2 Mean and variance of infrasound arrival parameters at WBCI during streamer events and on calm days and number of detection families.

	mean	variance	number of detections
RMS amplitude [Pa], calm days	0.013	< 0.001	11343
RMS amplitude [Pa], streamer event 3-7 November 2020	0.077	0.001	482
RMS amplitude [Pa], streamer event 21-25 November 2020	0.024	< 0.001	360
RMS amplitude [Pa], streamer event 9-12 March 2021	0.013	< 0.001	1543

Table 3 Mean and variance of the RMS amplitude and number of detections at PVCI in the set of calm days and during the respective streamer events.

References

Assink, J.D., Waxler, R., Smets, P., Evers, L.G. (2014). Bidirectional infrasonic ducts associated with sudden stratospheric warm-ing events. J. Geophys. Res. Atmos. 119,1140-1153.

Bittner, M., Höppner, K., Pilger, C., Schmidt, C. (2010). Mesopause temperature perturbations caused bzy infrasonic waves as a potential indicator for the detection of tsunamis and other geo-hazards. Nat. Hazards Earth Syst. Sci., 10, 1431-1442. www.nat-hazards-earth-syst-sci.net/10/1431/2010/doi:10.5194/nhess-10-1431-2010

Blanc, E. (1985). Observations in the upper atmosphere of infrasonic waves from natural or artificial sources: A summary. Ann. Geophys., 3, 673-688.

Blixt, E.M., Nasholm, S.P., Gibbons, S.J., Evers, L.G., Charlton-Perez, A.J., Orsolini, Y.J., Kvaerna, T. (2019). Estimating tropo-spheric and stratospheric winds using infrasound from explosions. J. Acoust. Soc. Am. 146:2.

Blom, P., Waxler, R. (2012). "Impulse propagation in the nocturnal boundary layer: Analysis of the geometric component". *J. Acoust. Soc. Am.*, **131**, 3680 – 3690. doi: 10.1121/1.3699174.

Blom, P. (2019). "Modeling infrasonic propagation through a spherical atmospheric layer: Analysis of the stratospheric pair." *J. Acoust. Soc. Am.*, **145**, 2198–2208. doi: 10.1121/1.5096855.

Bondár I., T. Šindelářová, D. Ghica, U. Mitterbauer, A.Liashchuk, J. Baše, J. Chum, C. Czanik, C. Ionescu, C. Neagoe, M. Pásztor, A. Le Pichon (2022), Central and Eastern European Infrasound Network: Contribution to Infrasound Monitoring, *Geophys. J. Int.*, ggac066, https://doi.org/10.1093/gji/ggac066

Brachet, N., Brown, D., Le Bras R., Cansi, Y., Mialle, P., Coyne, J. (2010). Monitoring the Earth's Atmosphere with the Global IMS Infrasound Network. In: Le Pichon, A., Blanc, E., Hauchecorne A. (Eds.), Infrasound Monitoring for Atmospheric Studies. Springer Science+Business Media B.V., 77-118. Doi: 10.1007/978-1-4020-9508-5_3

~~Bondár I., T. Šindelářová, D. Ghica, U. Mitterbauer, A.Liashchuk, J. Baše, J. Chum, C. Czanik, C. Ionescu, C. Neagoe, M. Pásztor, A. Le Pichon (2022), Central and Eastern European Infrasound Network: Contribution to Infrasound Monitoring, *Geophys. J. Int.*, ggac066, https://doi.org/10.1093/gji/ggac066~~

Campus, P., Christie, D.R. (2010). Worldwide Observations of Infrasonic Waves. In: Le Pichon, A., Blanc, E., Hauchecorne A. (Eds.), Infrasound Monitoring for Atmospheric Studies. Springer Science+Business Media B.V., 185234-118. Doi: 10.1007/978-1-4020-9508-5_6

Cansi, Y., 1995. An automatic seismic event processing for detection and location: The P.M.C.C. method. Geophys. Res. Lett. 22, 1021-1024. doi: 10.1029/95GL00468

Ceranna, L., Matoza, R., Hupe, P., Le Pichon, A., Landès, M., (2019). Systematic Array Processing of a Decade of Global IMS Infrasound Data. In: Le Pichon, A., Blanc, E., Hauchecorne, A. (eds) Infrasound Monitoring for Atmospheric Studies. Chal-lenges in Middle Atmospheric Dynamics and Societal Benefits. Springer Nature Switzerland AG.

Chum J, Podolská K (2018) 3D analysis of GW propagation in the ionosphere. Geophysical Research Letters, 45, 11,562–11,571, https://doi.org/10.1029/2018GL07969

Chum, J., Podolská, K., Rusz, J., Baše, J., Tedoradze, N. (2021), Statistical investigation of gravity wave characteristics in the ionosphere. Earth Planets Space 73, 60, ~~https://doi.org/10.1186/s40623-021-01379-3~~https://doi.org/10.1186/s40623-021-01379-3

Czech microbarograph network, https://doi.org/10.7914/SN/C9

Drob, D. P., Picone, J. M., Garcés, M. (2003). Global morphology of infrasound propagation. *J. Geophys. Res. Atmospheres*, **108** (D21). doi: 10.1029/2002JD003307.

Evers, L. G., Siegmund, P. (2009). Infrasonic signature of the 2009 major sudden stratosphericwarming, Geophys. Res. Lett., 36, L23808, doi:10.1029/2009GL041323

Evers, L.G., Haak, H.W. (2010). The Characteristics of Infrasound, its Propagation and Some Early History. In: Le Pichon, A., Blanc, E., Hauchecorne, A. (eds) Infrasound Monitoring for Atmospheric Studies. Springer, Dordrecht.

Evers, L. G., van Geyt, A. R. J. , Smets, P., Fricke, J.T. (2012). Anomalous infrasound propagation in a hot stratosphere and the existence of extremely small shadow zones, J. Geophys. Res., 117, D06120, doi:10.1029/2011JD017014.

Eyring, V., Dameris, M., Grewe, V., Langbein, I., & Kouker, W. (2002). Climatologies of streamer events derived from a transport model and a coupled chemistry-climate model.

Fritts, D.C. & Alexander, M.J., (2003). Gravity wave dynamics and effects in the middle atmosphere. Rev. Geophys., 41 (1), 1003.

Garcès, M., Willis, M., Hetzer, C., Le Pichon , A., Drob, D., (2004). On using ocean swells for continuous infrasonic measurements of winds and temperature in the lower, middle, and upper atmosphere. Geophys. Res. Lett. 31, L19304. doi: 10.1029/2004GL020696

Garcès, M.A., (2013). On infrasound standards, part 1: Time, frequency, and energy scaling. InfraMatics 2, 13-35. doi: 10.4236/inframatics.2013.22002

Georges, T.M. (1968). H. F. Doppler studies of travelling ionospheric disturbances. J. Atmos.Terr. Phys., 30, 735-746.

Gerlach, C., Földvary, L., Švehla, D., Gruber, T., Wermuth, M., Sneeuw, N., ... & Steigenberger, P. (2003). A CHAMP-only gravity field model from kinematic orbits using the energy integral. Geophysical Research Letters, 30(20).

Hersbach, H., Bell, B., Berrisford, P., Hirahara, S., Horányi, A., Muñoz-Sabater, J., ... & Thépaut, J. N. (2020). The ERA5 global reanalysis. Quarterly Journal of the Royal Meteorological Society, 146(730), 1999-2049.

Hupe, P., Ceranna, L., ~~Hupe, Patrick, Lars Ceranna, and Christoph Pilger. (2018). "Using barometric time series of the IMS infrasound network for a global analysis of thermally induced atmospheric tides." *Atmospheric Measurement Techniques* 11.4 2027-2040.~~

Pilger, C., de Carlo, M., Le Pichon, A., Kaifler, B., Rapp, M. (2019). Assessing middle atmosphere weather models using infrasound detections from microbaroms. Geophys. J. Int., 216, 1761–1767 doi: 10.1093/gji/ggy520

James, P. M. (1998): A climatology of ozone mini-holes over the Northern Hemisphere. International Journal of Climatology: A Journal of the Royal Meteorological Society, 18, 12: 12871303

Kramer, R, S. Wüst, and M. Bittner (2016). Investigation of gravity wave activity based on operational radiosonde data from 13 years (1997-2009): Climatology and possible induced variability, Journal of Atmospheric and Solar-Terrestrial Physics 140, 23–33; http://dx.doi.org/10.1016/j.jastp.2016.01.014

Kramer, R., S. Wüst, C. Schmidt, and M. Bittner (2015). Gravity wave characteristics in the middle atmosphere during the CESAR campaign at Palma de Mallorca in 2011/2012: Impact of extratropical cyclones and cold fronts, Journal of Atmospheric and Solar-Terrestrial Physics 128 (2015) 8–23, http://dx.doi.org/10.1016/j.jastp.2015.03.001

Kai Ming Huang, Shao Dong Zhang, Fan Yi, (2010).Reflection and transmission of atmospheric gravity waves in a stably sheared horizontal wind field, Journal of Geophysical Research: Atmospheres, 10.1029/2009JD012687, **115**, D16,

Landès, M., Ceranna, L., Le Pichon, A., & Matoza, R. S. (2012). Localization of microbarom sources using the IMS infrasound network. Journal of Geophysical Research: Atmospheres, 117(D6).

Le Pichon, A., Cansi, Y. (2003). PMCC for infrasound data processing. InfraMatics 02, 1-9.

Le Pichon, A., Blanc, E., (2005). Probing high-altitude winds using infrasound. J. Geophys. Res., 110, D20104. doi: 10.1029/2005JD006020

Le Pichon, A., Ceranna, L., Garcès, M., Drob, D., Millet, C., (2006). On using infrasound from interacting ocean swells for global continuous measurements of winds and temperature in the stratosphere. J. Geophys. Res., 111, D11106. doi: 10.1029/2005JD006690

Le Pichon, A., Vergoz, J., Blanc, E., Guilbert, J., Ceranna, L., Evers, L., Brachet, N., (2009). Assessing the performance of the International Monitoring System's infrasound network: Geographical coverage and temporal variabilities. J. Geophys. Res. 114, D08112. doi: 10.1029/2008JD010907

Le Pichon, A., Ceranna, L., Vergoz, J. (2012). Incorporating numerical modelling into estimates of the detection capability of the IMS infrasound network. J. Geophys. Res., 117, D05121. doi: 10.1029/2011JD016670

Leovy, C. B., Sun, C. R., Hitchman, M. H., Remsberg, E. E., Russell III, J. M., Gordley, L. L., ... & Lyjak, L. V. (1985). Transport of ozone in the middle stratosphere: Evidence for planetary wave breaking. Journal of Atmospheric Sciences, 42(3), 230-244.

Lonzaga, J.B., (2015). A theoretical relation between the celerity and trace velocity of infrasonic phases, J. Acoust. Soc. Am., 138, EL242-EL247. http://dx.doi.org/10.1121/1.4929628

Loyola D.G., Koukouli M.E., Valks P., Balis D.S., Hao N., van Roozendael M., Spurr R.J.D., Zimmer W., Kiemle S., Lerot C., Lambert J.-C. (2011) The GOME-2 total column ozone product: Retrieval algorithm and ground-based validation, Journal of Geophysical Research, vol. 116, D07302, Wiley-Blackwell

Marty, J., (2019). The IMS Infrasound Network: Current Status and Technolofical Developments, in: Le Pichon, A., Blanc, E., Hauchecorn, A. (Eds.), Infrasound Monitoring for Atmospheric Studies. Challenges in Middle Atmosphere Dynamics and Societal Benefits. Springer Nature Switzerland AG, pp. 3–62. doi:10.1007/978-3-319-75140-5_1

McIntyre, M. E., & Palmer, T. N. (1983). Breaking planetary waves in the stratosphere. Nature, 305(5935), 593-600.

Munro, R., Eisinger, M., Anderson, C., Callies, J., Corpaccioli, E., Lang, R., ... & Albinana, A. P. (2006, June). GOME-2 on MetOp. In Proc. of The 2006 EUMETSAT Meteorological Satellite Conference, Helsinki, Finland (Vol. 1216, p. 48).

Munro, R., et al. (2016): The GOME-2 instrument on the Metop series of satellites: instrument design, calibration, and level 1 data processing – an overview, Atmos. Meas. Tech., 9, 1279–1301, https://doi.org/10.5194/amt-9-1279-2016.

Peters, D., Hoffmann, P., & Alpers, M. (2003). On the appearance of inertia-gravity waves on the north-easterly side of an anticyclone. Meteorologische Zeitschrift, 12(1), 25-35

Polvani, L. M., & Plumb, R. A. (1992). Rossby wave breaking, microbreaking, filamentation, and secondary vortex formation: The dynamics of a perturbed vortex. Journal of Atmospheric Sciences, 49(6), 462-476.

Pramitha, M., Venkat Ratnam, M., Taori, A., Krishna Murthy, B. V., Pallamraju, D., and Vijaya Bhaskar Rao, S. (2015). Evidence for tropospheric wind shear excitation of high-phase-speed gravity waves reaching the mesosphere using the ray-tracing technique, Atmos. Chem. Phys., 15, 2709–2721, https://doi.org/10.5194/acp-15-2709-2015.

Rauthe, M., Gerding, M., Höffner, J., & Lübken, F. J. (2006). Lidar temperature measurements of gravity waves over Kühlungsborn (54° N) from 1 to 105 km: A winter-summer comparison. Journal of Geophysical Research: Atmospheres, 111(D24).

Wüst, S., & Bittner, M. (2006). Non-linear resonant wave–wave interaction (triad): Case studies based on rocket data and first application to satellite data. Journal of atmospheric and solar-terrestrial physics, 68(9), 959-976.

Wüst, S., Offenwanger, T., Schmidt, C., Bittner, M., Jacobi, C., Stober, G., Yee, J.H., Mlynczak, M. G. & Russell III, J. M. (2018). Derivation of gravity wave intrinsic parameters and vertical wavelength using a single scanning OH (3-1) airglow spectrometer. Atmospheric Measurement Techniques, 11(5), 2937-2947.

Smets, P.S.M., Evers, L.G. (2014). The life cycle of a sudden stratospheric warming from infrasonic ambient noise observa-tions, J. Geophys. Res. Atmos., 119, 12,084-12,099

Spurr, R., Loyola, D., Heue, K. P., Van Roozendael, M., & Lerot, C. (2022). S5P/TROPOMI Total Ozone ATBD. Deutsches Zentrum für Luft- und Raumfahrt (German Aerospace Center), Weßling, Germany, Tech. Rep. S5P-L2-DLR-ATBD-400A.

Sutherland, L.C., Bass, H.E., (2004). Atmospheric absorption in the atmosphere up to 160 km. *J. Acoust. Soc. Am.*, 115, 1012–1032. https://doi.org/10.1121/1.1631937

Szuberla, C.A.L., Olson, J.V., (2004). Uncertainties associated with parameter estimation in atmospheric infrasound rays. J. Acoust. Soc. Am. 115, 253-258. doi: 10.1121/1.1635407

~~Leovy, C. B., Sun, C. R., Hitchman, M. H., Remsberg, E. E., Russell III, J. M., Gordley, L. L., ... & Lyjak, L. V. (1985). Transport of ozone in the middle stratosphere: Evidence for planetary wave breaking. Journal of Atmospheric Sciences, 42(3), 230-244.~~

~~McIntyre, M. E., & Palmer, T. N. (1983). Breaking planetary waves in the stratosphere. Nature, 305(5935), 593-600.~~

~~Peters, D., Hoffmann, P., & Alpers, M. (2003). On the appearance of inertia-gravity waves on the north-easterly side of an anticyclone. Meteorologische Zeitschrift, 12(1), 25-35~~

~~Polvani, L. M., & Plumb, R. A. (1992). Rossby wave breaking, microbreaking, filamentation, and secondary vortex formation: The dynamics of a perturbed vortex. Journal of Atmospheric Sciences, 49(6), 462-476.~~

~~Munro, R., Eisinger, M., Anderson, C., Callies, J., Corpaccioli, E., Lang, R., ... & Albinana, A. P. (2006, June). GOME-2 on MetOp. In Proc. of The 2006 EUMETSAT Meteorological Satellite Conference, Helsinki, Finland (Vol. 1216, p. 48).~~

Veefkind, J. P., Aben, I., McMullan, K., Förster, H., De Vries, J., Otter, G., ... & Levelt, P. F. (2012). TROPOMI on the ESA Sentinel-5 Precursor: A GMES mission for global observations of the atmospheric composition for climate, air quality and ozone layer applications. Remote sensing of environment, 120, 70-83.

Spurr, R., Loyola, D., Heue, K. P., Van Roozendael, M., & Lerot, C. (2022). S5P/TROPOMI Total Ozone ATBD. Deutsches Zentrum für Luft- und Raumfahrt (German Aerospace Center), Weßling, Germany, Tech. Rep. S5P-L2-DLR-ATBD-400A.

Munro, R., et al. (2016): The GOME-2 instrument on the Metop series of satellites: instrument design, calibration, and level 1 data processing – an overview, Atmos. Meas. Tech., 9, 1279–1301, https://doi.org/10.5194/amt-9-1279-2016.

Loyola D.G., Koukouli M.E., Valks P., Balis D.S., Hao N., van Roozendael M., Spurr R.J.D., Zimmer W., Kiemle S., Lerot C., Lambert J.-C. (2011) The GOME-2 total column ozone product: Retrieval algorithm and ground-based validation, Journal of Geophysical Research, vol. 116, D07302, Wiley-Blackwell